Aeroacoustics Conferences
20-23 May 2019, Delft, The Netherlands
25th AIAA/CEAS Aeroacoustics Conference

10.2514/6.2019-2667

On the Use of RANS-informed Analytical Models to Perform Broadband Rotor-Stator Interaction Noise Predictions

Danny Lewis*, Stéphane Moreau† and Marc Jacob‡
Laboratoire de Mécanique des Fluides et d'Acoustique, UMR CNRS 5509, Ecole Centrale de Lyon, Université de Lyon, 69134 Ecully CEDEX, France.

In 2018, a comprehensive data base of aerodynamic and acoustic measurements was obtained from a test campaign performed on the "ACAT1" Fan stage at the Universal Fan Facility for Acoustics (UFFA) of AneCom AeroTest (ACAT). The present paper describes a hybrid method coupling RANS simulations with analytical models to predict the broadband noise resulting from the interaction of the rotor wakes with the stator vanes, also named Rotor Stator Interaction (RSI) noise. Several operating points (approach, cutback and sideline) were tested on two different working lines (the Sea Level Static (SLS) working line and a Low Noise (LN) working line) on two configurations displaying different rotor-stator spacings (called Short Gap and Long Gap). The present study focuses on the Short Gap configuration, at approach condition on the SLS working line. The aerodynamic test data is directly compared with a Menter k-ω SST RANS simulation, which is in good agreement with the experimental performance parameters as well as with the hot-wire measurements in the interstage section. The acoustic power spectra computed from the microphone measurements are then compared with the broadband noise predictions performed using two analytical models representing the state of the art of analytical broadband RSI noise prediction: Hanson's model and Posson's model. The noise predictions obtained from these models recover quite faithfully the overall shape of the experimental acoustic power spectra. The absolute noise levels are underestimated by 1 to 5 dBs with respect to the measurements, depending on both the analytical model and the turbulence length scale estimation that are used. This underestimation can be attributed to the fact that some assumptions made within the analytical models may not be correct in the present configuration. Another explanation may be that there are other dominant noise sources that are responsible for the broadband noise production such as the rotor self noise. Installation effects in the experiment may also be responsible for these discrepancies.

I. Nomenclature

Acronyms

$ACAT1$	=	Fan rig.
HW	=	Hot Wire.
LE	=	Leading Edge.
LES	=	Large Eddy Simulation.
LN	=	Low Noise.
OGV	=	Outlet Guide Vane.
PWL	=	Acoustic Power Level.
RSI	=	Rotor Stator Interaction.
SDT	=	NASA Source Diagnostic Test.
SLS	=	Sea Level Static.
TE	=	Trailing Edge.

*PhD candidate, Ecole Centrale de Lyon, LMFA, danny.lewis@ec-lyon.fr,.
†Professor, Ecole Centrale de Lyon, LMFA, AIAA Lifetime Member.
‡Professor, Ecole Centrale de Lyon, LMFA, AIAA Member.

TI = Turbulence Intensity.
TKE = Turbulence Kinetic Energy.
TLS = Turbulence Length Scale.
WND = Wave Number Decomposition.

Mathematical symbols

h = Order of Fourier mode.
p' = Pressure fluctuation.
v_x, v_{theta}, w_{rad} = Fluctuations of the axial, circumferential and radial components of the velocity.
V_x, V_{theta}, V_{rad} = Axial, circumferential and radial components of the velocity.

subscripts

rms = Root mean square.
1 = Pope estimate (int. length scale).
2 = Jurdic estimate (int. length scale).

II. Introduction

In order to simultaneously maintain airport development and a viable environment in their vicinity, companies involved in aircraft manufacturing have come together to address the question of noise pollution. Significant engine noise reductions have already been achieved, especially through the increase in the bypass ratio which led to a substantial decrease in the jet noise. The tonal contribution of the noise has also been decreased by cleverly selecting the number of blades and vanes in the engines, and by using passive noise control technologies such as acoustic liners. Currently, engine manufacturers are planning to move from High Bypass Ratio (HBR) architectures, with a bypass ratio between 10 and 12, to Ultra High Bypass Ratio (UHBR) architectures, the bypass ratios of which are between 15 and 20. In this type of configuration, the Fan-OGV (Outlet Guide Vane) stage becomes a major contributor to the total radiated noise which is expected to be dominated by the broadband noise contribution. Thus, there is a substantial interest in reducing this contribution.

Fan broadband noise results from multiple random fluctuating mechanisms such as turbulence ingestion at the inlet, the turbulent boundary layers, the tip vortex and the wakes. The main mechanism responsible for the broadband noise production is however the rotor-stator interaction (RSI) noise which results from the interaction between the rotor turbulent wakes and the stator, generating loading fluctuations on the vanes and eventually producing both tonal and broadband noise. The present study focuses exclusively on the broadband part of this interaction. Due to its prohibitive CPU cost, performing Direct Numerical Simulations (DNS) to study the RSI noise is still inconceivable to simulate RSI noise in the industrial context. Therefore, new methods have to be developed to predict noise at a lower cost. Three alternatives to DNS currently represent the state of the art of RSI broadband noise prediction:

1) Analytical models: this method couples a CFD computation with an analytical model. Flow parameters are extracted from the simulation (RANS or LES) and are used as inputs for the analytical model. The model then computes the unsteady loading on the vane and uses it as an equivalent dipole source within an acoustic analogy[1–3]. The advantage of this approach is that it requires only flow computations using statistical turbulence models (RANS, URANS), the flow unsteadiness being modeled based on assumptions about the wake turbulence. Its weakness is precisely due to the limitations of these flow models and the required vane and duct geometry simplifications. The combination of LES with these models allows to refine the unsteady flow information.
2) Hybrid methods: they couple a CFD computation with a numerical propagation method. The two following approaches represent the state of the art of hybrid methods. The main difference between the two lies in the approach undertaken to compute the wave propagation:
    1) Propagation using acoustic analogies [1] : the noise sources are directly computed in a compressible Large Eddy Simulation and are then coupled with an acoustic analogy such as the Ffowcs Williams

and Hawkings [4] free field analogy, or the Goldstein [5] duct analogy to recover the acoustic far field. Their advantage is that the sources are accurately modeled if the unsteady flow computation is carried out carefully. Their main drawback is that the Green's function is only known for canonical geometries (free-field, uniform flow, annular cylindrical ducts, with possible but complex extensions to slowly varying ducts, lined ducts, mean swirl flows... but not to shear flows for instance).

2) Propagation using Linearized Euler Equations (LEE)[6] : this method is a two step calculation which decouples the sound generatd by turbulence from its propagation. In the first step, a mean flow field is computed by solving the RANS equations and the Euler's equations are then linearized around this mean flow. In a second step, the LEE are solved with an additional turbulent source term which is referred to as the synthetic turbulence model [7, 8]. This source may be a stochastic model which is used to synthesize the velocity turbulence field which will be propagated. This approach is very attractive since it allows taking into account mean shear as well as the actual geometry. However, besides the underlying assumption about the turbulence required for the source modeling, which could be avoided if it were coupled with unsteady CFD (LES, LBM), its main drawback is that it may become extremely expensive for complex geometries and high frequencies such as those encountered in fan-OGV broadband cases.

3) Direct noise propagation using the Lattice-Boltzmann Method (LBM): thanks to reduced CPU costs, at moderate Mach numbers, and the low dissipation of the method, direct broadband noise simulations have recently been achieved using LBM. LBM is a promising alternative to LES, but its applicability to high speed compressible flows such as those encountered in fan-OGV computations is still limited, in particular because of the high computational costs it then requires.

The objective of the present paper is to assess the capacity of the first method to provide reliable predictions of broadband RSI noise. The CFD computation as well as the broadband noise predictions are all performed on the ACAT1 configuration that was recently tested in the ANECOM UFFA facility in Wildau (Germany) in the framework of the European project TurbonoiseBB.

III. Benchmark Configuration

The ACAT1 turbofan model consists of 20 fan blades and of 44 stator vanes. Two configurations were tested: one with a short inter-stage and an additional one with a longer inter-stage. Both configurations were tested at different operating conditions (approach, side-line and cut-back condition) on two different working lines (SLS and LN) which differ by the blade loading of the fan. The present paper focuses exclusively on the SLS working line, at approach condition, for the short inter-stage configuration. The flow conditions of this operating point are given in Table 1.

Rotation speed (rpm)	3828.2
Total mass-flow rate (kg/s)	55.156
Bypass ratio	7.6
Ambient pressure (hPa)	995.6
Ambient temperature (K)	292.8
Turbulence intensity at the inlet (%)	0.3
Turbulence length-scale at the inlet (m)	0.04

Table 1 Approach condition.

IV. Simulation Set-Up

A. Computational Domain

The meridional view of the computational domain is depicted in Fig. 2. The computational domain extends from 4 fan axial chords upstream of the rotor to 6 vane axial chords downstream of the stator. For the RANS computation

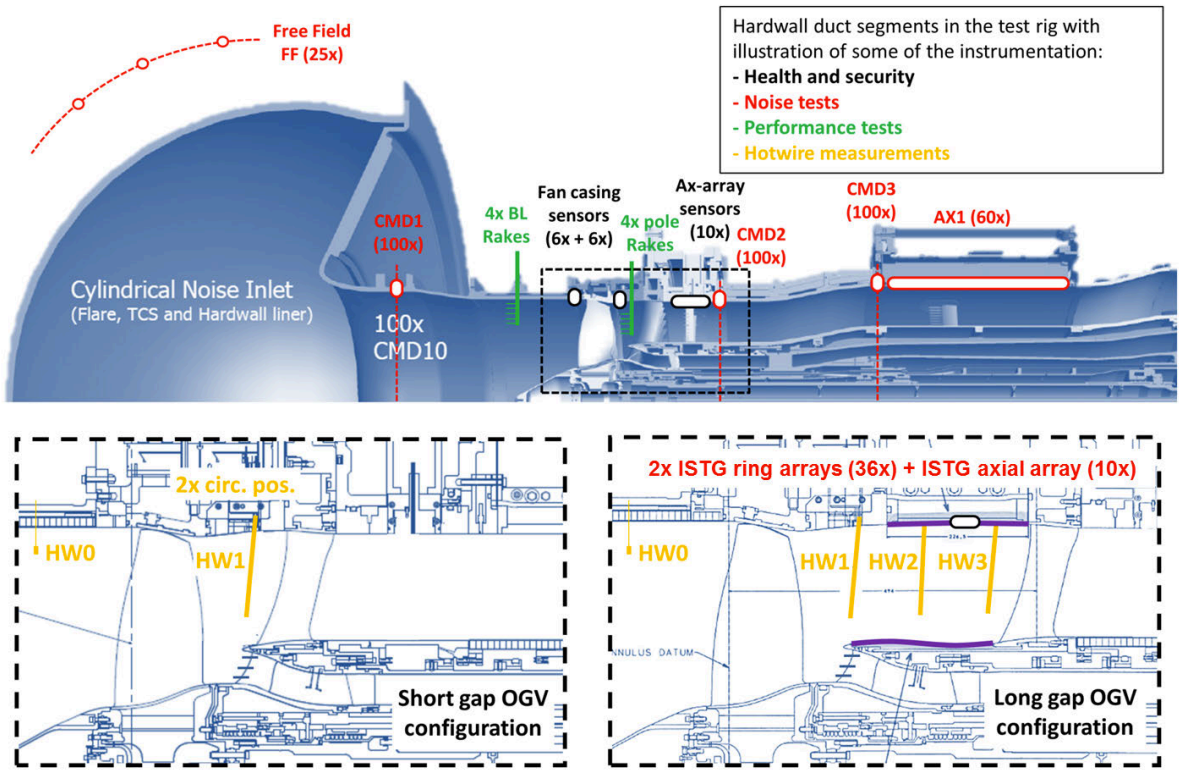

Figure 1 View of the UFFA fan rig of AneCom AeroTest. Ring arrays were used for acoustic measurements at the inlet (CMD1), interstage (ISTG) and bypass (CMD3) sections, and axial arrays at the interstage and in the by-pass duct. Moreover, an array of 25 microphones, equally distributed from 0 to 120 degrees along an arc of radius 18.5 m centered on the fan axis at the nozzle inlet, was used for far field sound measurements upstream of the inlet.

described herein, it has been reduced to one rotor passage and one stator passage by the use of periodic boundary conditions. Since the objective of this paper is to study the Fan-OGV interaction, the Inlet Guide Vane (IGV) in the core flow has been removed to build the computational domain, making it possible to focus the mesh refinements on the zones of interest.

B. Unstructured Mesh

The mesh is a hybrid unstructured grid composed of prism cells on walls, to accurately resolve the boundary layer, and of tetrahedral cells in the rest of the domain. Volume and surface refinements are introduced (see Fig. 3 and Fig. 4) in order to ensure the quality of the mesh. Surface refinements are mainly used to accurately discretize the blades and the vanes, especially the leading edges (LE), the trailing edges (TE) and the fillets. Four main refinement blocks are used on both the fan and the OGV:

- Wake refinements to correctly transport the wakes.
- LE and TE refinements to ensure a smooth transition from the coarse to the fine mesh near the walls.
- Tip-gap refinements.
- Inter-blade region refinements to guarantee a correct azimuthal description of the flow.

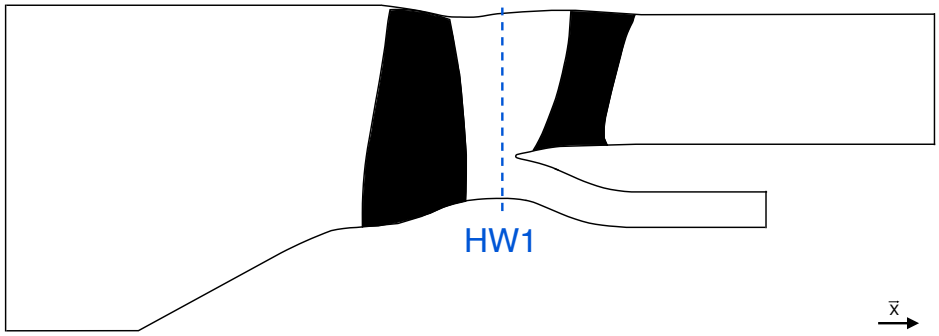

Figure 2 Computational domain.

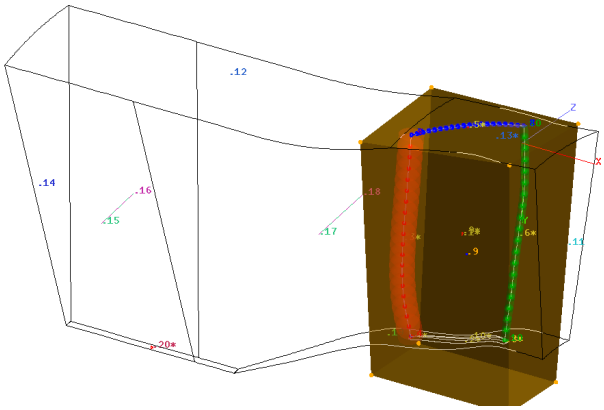

Figure 3 Rotor-blade refinement blocks.

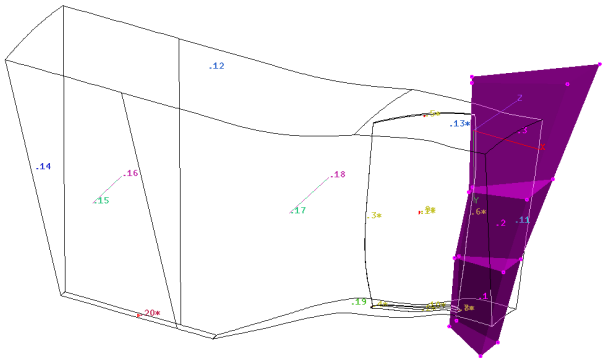

Figure 4 Rotor wake refinement blocks.

The final mesh displayed in Figs. 5, 6 and 7 is the result of a mesh-convergence study that has needed several iterations.

These parameters eventually lead to a mesh composed of 50 million cells in the rotor domain and of 20 million cells in the stator domain. The significant oversizing of the mesh is mainly due to the wake-refinement blocks which have been chosen excessively large to guarantee that the mesh follows the wakes. Consequently, a significant number of cells generated for the wake is actually not within the simulated wake. In addition, the use of such volume refinements creates cells that are almost isotropic, which significantly increases the number of cells in the wake compared to a structured mesh. The use of a refinement block fitted to the wake would have reduced the mesh size almost by half. However, since the computational cost of RANS computations is quite low, no mesh optimization aiming at reducing its size was conducted. In terms of mesh quality the equivolume skewness has been maintained below 1, which guarantees that there are no degenerate cells. Similarly, the equiangle skewness is kept below 0.95, which is the limit of sliver cells.

C. RANS Simulation

The RANS simulation has been performed using the code ANSYS CFX v19.2. The high resolution CFX convection scheme has been used with Menter's k-ω SST turbulence model. The dimensionless mesh size, y^+, is close to 1 on the casing and maintained below 1 on the blades and vanes in order to fully resolve the boundary layer. The convergence of the simulation has been checked monitoring both RMS values of the residuals and the convergence of key variables (mass-flow rates, pressure ratio).

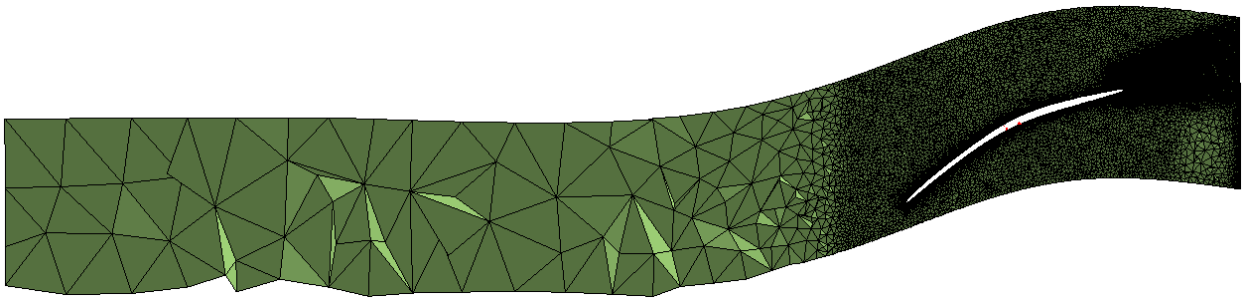

Figure 5 Mesh midspan radial cut of the rotor domain.

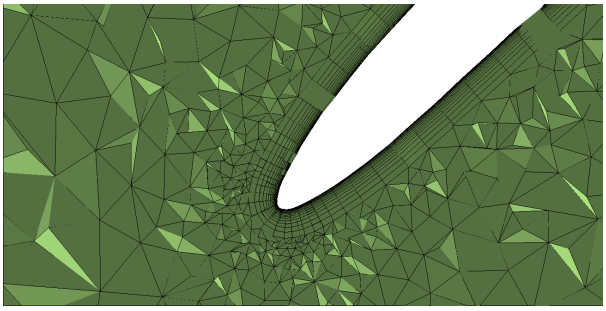

Figure 6 Rotor-blade LE mesh.

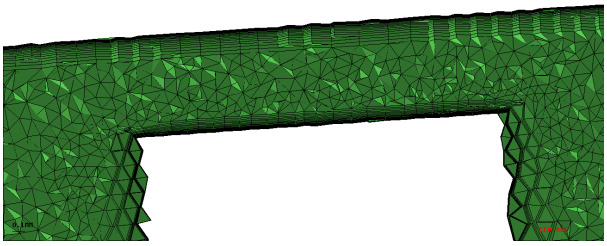

Figure 7 Rotor-blade tip-gap mesh.

V. Aerodynamic Analysis

The results obtained from the RANS simulation are presented in the following sections. Results are compared to both the performance parameters and the HW measurements at position HW1.

A. Performance Parameters

Table 2 presents the performance parameters at approach condition obtained from the RANS computation. These values were obtained from a mass-flow rate weighted average over an axial field cut at the splitter location, upstream of the stator. The agreement of the RANS results with the experimental data is excellent within the measurement uncertainty: the computed bypass pressure ratio is close to the experimental value (0.36% error) as well as the pressure ratio of the core flow (0.2% error). The total fan pressure ratio (FPR), computed from the mass-flow rate weighted average of the core and bypass FPR, is close to the experimental data.

	Massflow rate (kg/s)			Fan pressure ratio		
	Bypass	Core	Total	Bypass	Core	Total
Experiment	55.156	6.411	48.745	1.110	1.100	1.109
RANS	55.156	6.411	48.745	1.106 (−0.36%)	1.098 (−0.2%)	1.105 (−0.34%)

Table 2 Performance parameters obtained from the RANS simulation at approach condition.

B. Mean Flow

1. Friction Lines Analysis

At approach condition, the fan is operating at higher angles of attack than at cruise condition. This commonly results in local flow separations. Flow detachments are usually tracked by looking at the friction lines on the blade surface. Figure 8 shows the fan suction side colored by the axial component of the friction vector with the corresponding friction lines. As expected, a LE flow separation appears from 20% of the fan height up to the tip of the rotor. The flow reattaches before reaching half of the blade chord and remains attached down to the TE. Regarding the vane (Fig. 9), the flow remains attached on almost all the suction side surface. Small separation zones appear at the LE close to the casing and at the TE at 10% of the vane height.

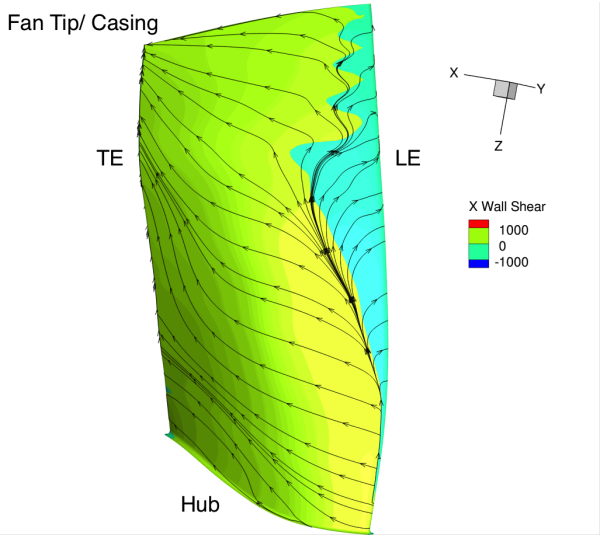

Figure 8 Friction lines on the fan suction side.

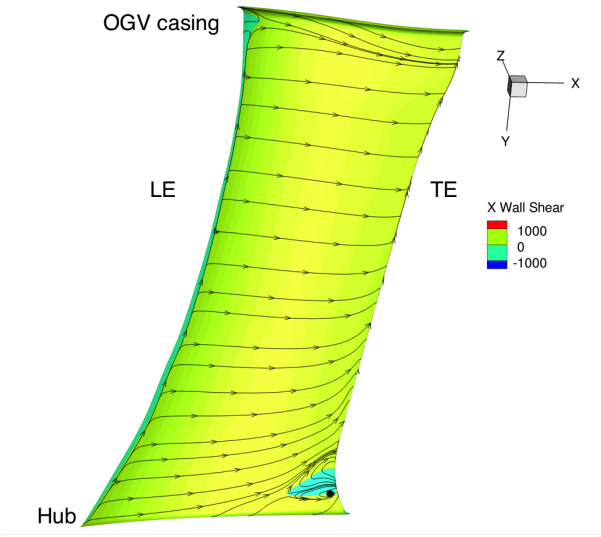

Figure 9 Friction lines on the vane suction side.

2. Fan Wake Analysis

Since broadband interaction noise results from the impingement of turbulent structures onto the vanes, analytical models for broadband noise prediction rely heavily on turbulence data. In particular, data related to the wake turbulence (turbulent kinetic energy and dissipation) and to the characteristic dimensions (wake width, integral length scale) need to be accurately predicted in order to perform reliable noise predictions. As a consequence, it is of paramount importance to ensure that the wakes are sufficiently discretized and properly convected through the domain. Axial cuts at hot-wire HW1 location (X=-2.685m, see Fig. 2) showing the axial velocity field and the turbulent kinetic energy (TKE) are displayed in Figs. 10 and 11. It can be observed that from 20% of the rotor height up to the tip of the rotor, the wakes progressively thicken and the turbulent kinetic energy intensifies. The previously mentioned LE flow separation that covers the same span area seems to be responsible for this phenomena, creating disturbances in the flow, which eventually leads to higher levels of TKE.

Figures 12, 13, 14 and 15 compare the 2D maps of the velocity components and the TKE from the HW measurements to those from the RANS simulation.

The RANS simulation overestimates the value of the axial velocity in the inter-blade zone, whether it is in the bypass or the core flow (see Fig. 12). However, the axial velocity predicted by the RANS simulation within the wake is lower than what is observed experimentally, resulting in an even larger wake deficit in the RANS computation. The overall shape of the wake is well predicted by the RANS simulation in terms of wake thickness and tilting. However, the tip-gap vortex seems to be more important in the experiment and the casing boundary layer is thinner than in the RANS simulation. The circumferential velocity is in good agreement with the experiment, with a slight overestimation from the hub up to 20% of the rotor span. The radial component of the velocity, however, displays significant discrepancies

with the experiment, especially in the intermediate zone between the core and the bypass flow where the magnitude is overestimated by almost 9 m/s. The same range of discrepancies has been observed by Guerin *et al.*[9] which may infer that these disparities might be attributed either to the RANS as such or even to the experimental values. At this point it must be pointed out that the radial velocity is significantly smaller (by about one order of magnitude) than the main azimuthal and axial velocity components : therefore it is prone to large variations from one configuration or operating point to another very close one or, equivalently, to relative errors between measurements and computations.

Figures 15a and 15b show the TKE from the experiment and the RANS simulation respectively. The TKE from the experiment was computed using $TKE = \frac{1}{2} * (v^2_{x,rms} + v^2_{theta,rms} + w^2_{rad,rms})$ whereas the RANS TKE is basically the k variable from the k-ω SST turbulence model. A significant overestimation can observed for the RANS TKE with TKE levels that are almost twice as high as the experimental levels. The substantial LE flow detachment observed on the rotor in the RANS simulation cannot be clearly identified when looking at the HW measurements, except on isolated wakes (at 12, 2 and 3 o'clock for instance). This may imply that this phenomenon might not be as important in the experiment as it is in the simulation.

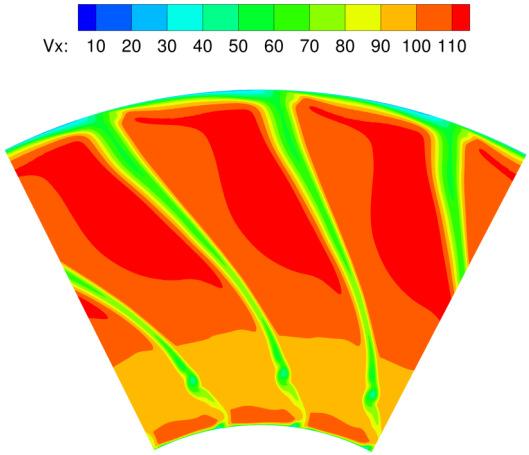

Figure 10 Axial velocity field, RANS results at position HW1.

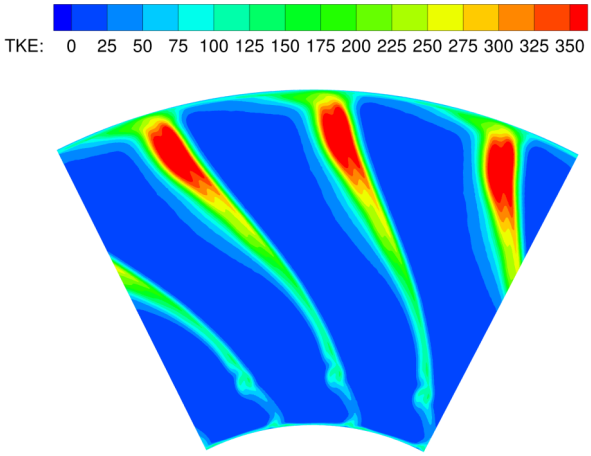

Figure 11 Turbulent Kinetic Energy field, RANS results at position HW1.

VI. Broadband Noise Predictions Using Analytical Models

A. Wake Extrapolation

In order to predict broadband noise using the analytical models, flow data has to be extracted from a CFD simulation. This extraction must be performed on a plane as close as possible to the LE of the vane to guarantee that it is representative of the flow impinging upon the vane cascade. A RANS simulation at approach condition has been carried out using the mixing plane approach. The mixing plane was located halfway between the rotor and the stator, 6 mm upstream of the splitter. As a consequence, since the mixing plane performs an azimuthal average of the flow, the wakes can only be extracted upstream of it. Performing broadband noise predictions based on input parameters extracted this far from the vane would inevitably lead to overestimated predictions since the models would have been informed with flow parameters (turbulent intensity and integral length scale) that have not decayed enough. To overcome this issue, wake extrapolation methods have been developed. They enable to extrapolate the wakes up to the LE of the stator, increasing the reliability of the noise predictions. Leonard *et al.*[1] developed such an extrapolation method based on a Fourier series decomposition which proved to give fairly precise results. Jaron *et al.*[10] developed a method based on physical considerations which takes into account the potential field due to the rotor.

In order to reconstruct the wake information at the stator LE, the flow has been extracted at 200 axial positions from

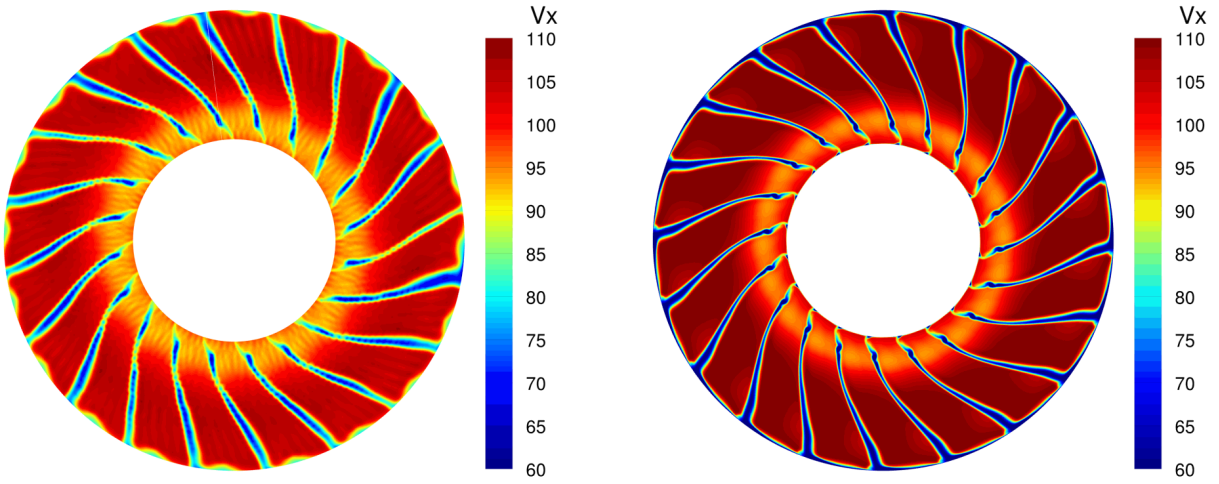

(a) HW measurements. **(b) RANS.**

Figure 12 Axial velocity field at position HW1.

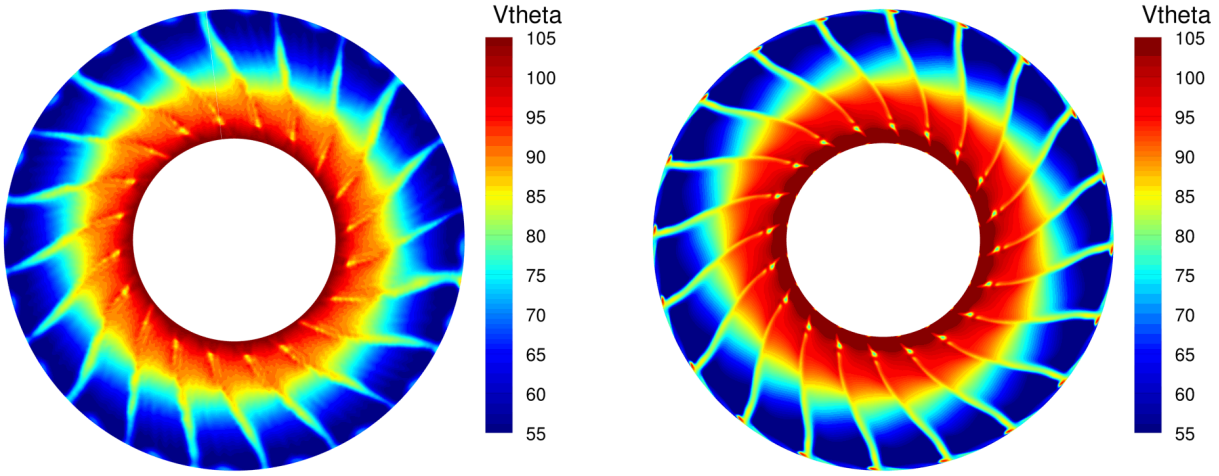

(a) HW measurements. **(b) RANS.**

Figure 13 Circumferential velocity field at position HW1.

the rotor TE up to the mixing plane. For each axial cut, the wake profile has been extracted on 120 radial positions and 320 azithumal positions. Each azimuthal profile is then fitted using a Fourier series decomposition with a maximum of 9 harmonics.

For each radial position, the axial evolution of the phase and amplitude coefficients of the velocity components has been fitted using Jaron's method. Since the method of Jaron is neither dedicated to the TKE (k variable of the Menter SST model) nor to the turbulence eddy frequency (ω variable of the Menter SST model) extrapolations, the axial evolution of their Fourier coefficients has been fitted with a mean square method to a sum of two exponential functions for the amplitude (typical for a diffusive process), and a linear function for the phase (consistent with a constant convection velocity).

The Fourier coefficients are then extrapolated down to the stator LE based on these fitting functions (see Fig. 16) and used to reconstruct the 2D map of the wake at this position (Figs. 17 and 18).

Figure 16 shows that the extrapolations fit very closely the extracted values in the region where both data are

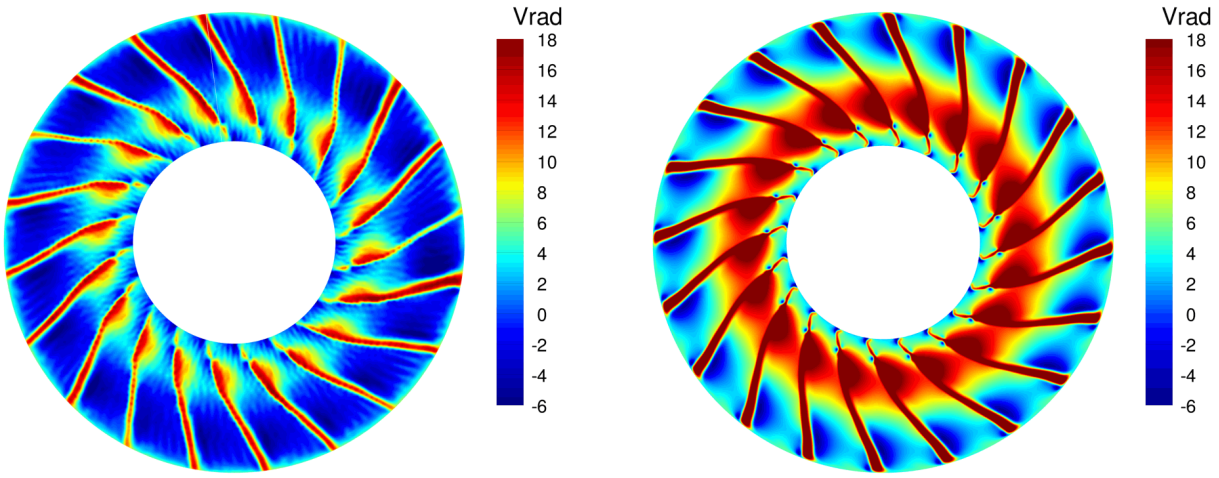

(a) HW measurements. **(b) RANS.**

Figure 14 Radial velocity field at position HW1.

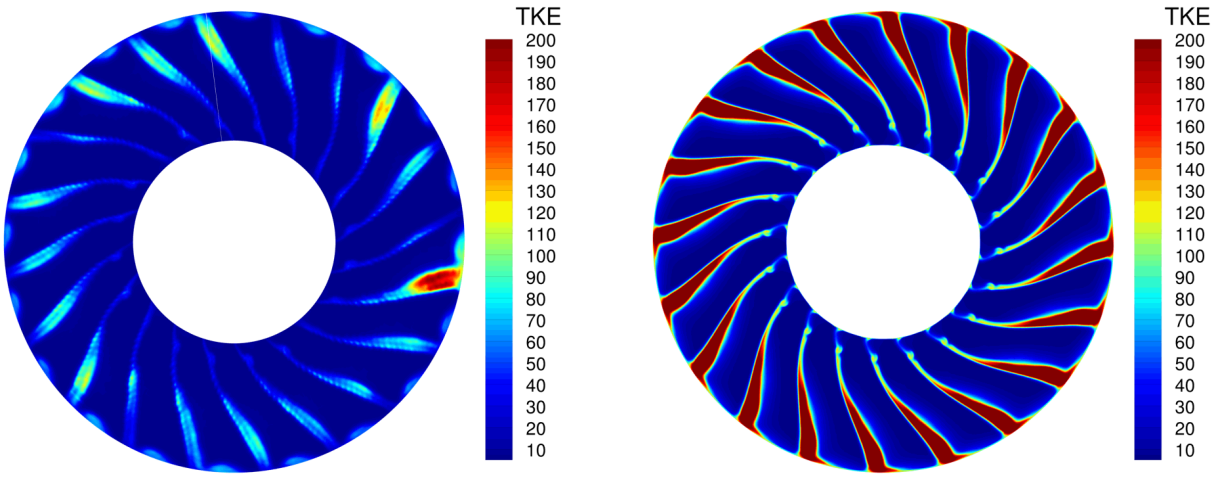

(a) HW measurements. **(b) RANS.**

Figure 15 Turbulent Kinetic Energy at position HW1.

available, which gives some confidence to the downstream region where the extrapolation stands alone. In fact the fitting is very satisfactory over the whole blade span, except for radii very close to the hub and the casing where the boundary layer prevented the fitting from being as accurate as in the rest of the domain, for all harmonics. The hub part of the wake is not an issue in our case since it is extrapolated into the core flow. However, as it can be seen is Figs 17 and 18, the flow near the casing seems to be impacted by this phenomenon since small discontinuities appear.
The validation of this extrapolation against experimental data cannot be conducted since no HW measurements were performed at the stator LE. However, it can be noticed that the expected behavior of the wake seems to be well recovered: as expected, the velocity deficit due to the wakes is lower than at HW1 position and the extent of the wake has also been increased in the azimuthal direction (wake broadening). The TKE in the wake has significantly decreased whereas the background turbulence has slightly increased, especially above 50% of the stator span. The extrapolation also recovers the increased tilting of the wakes due to the swirl created downstream of the fan.

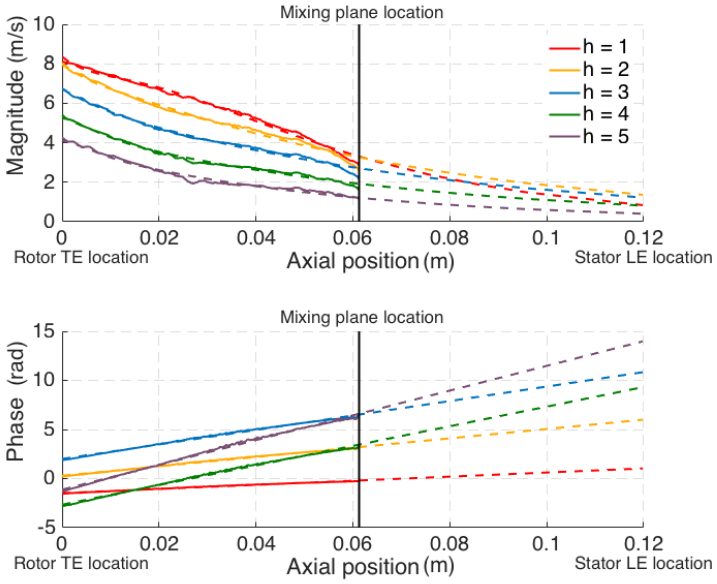

Figure 16 Fourier decomposition of the 5 first harmonics (h) of the axial velocity at rotor mid span: extracted values (solid lines) and extrapolated values (dashed lines).

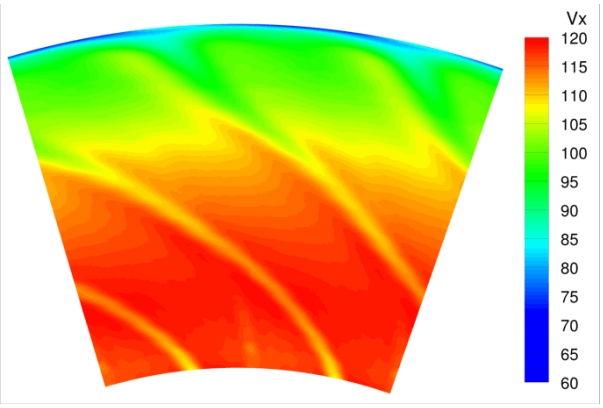

Figure 17 Reconstructed axial velocity field at the stator LE.

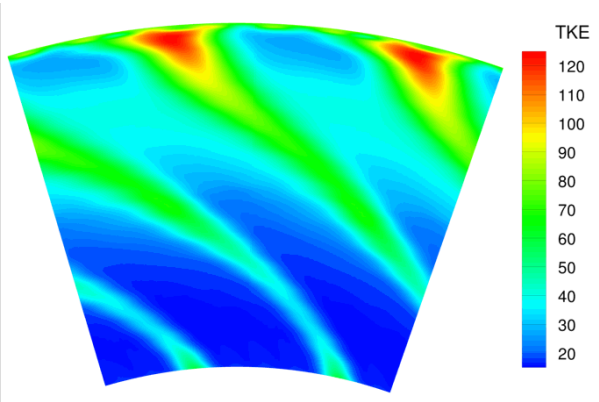

Figure 18 Reconstructed TKE field at stator LE.

B. Extraction of Inputs for Acoustic Models

Several input parameters need to be extracted from this extrapolation to predict the noise with analytical models:

- The axial velocity.
- The absolute velocity.
- The turbulence intensity (TI) in the wake and the background flow
- The turbulence length scale (TLS) in the wake and the background flow.
- The wake half width.

To extract these parameters, a Gaussian shape for the wake based on the absolute velocity and the turbulent kinetic energy (TKE) is assumed. A Gaussian fit is then performed on the wake retrieved from the simulation, separating the

background from the wake variables by applying a 20% threshold on the Gaussian wake (Fig. 19).

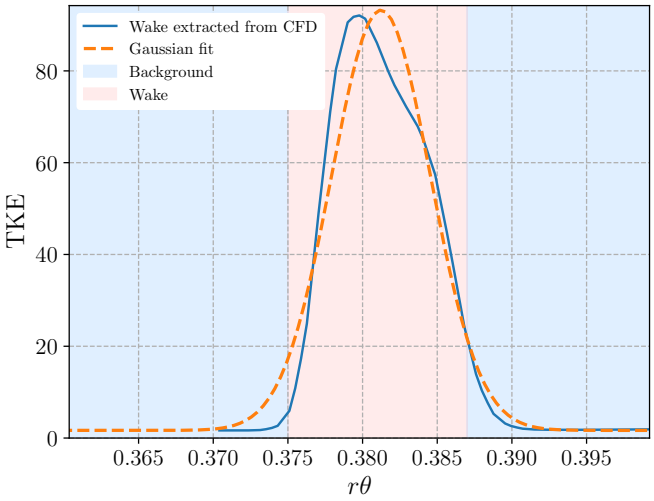

Figure 19 Wake extraction using a Gaussian fit.

There are several ways of estimating the streamwise integral length scale when using data retrieved from RANS simulations. The first one, proposed by Pope [11], makes direct use of the turbulent variables k and ω through the following relationship:

$$\Lambda_1 = 0.43\frac{\sqrt{k}}{C_\mu \omega} \tag{1}$$

with $C_\mu = 0.09$. Another estimate can be obtained using the wake width L_w with the empirical relationship of Jurdic *et al.*[12] :

$$\Lambda_2 = 0.21 L_w \tag{2}$$

For the latter relation, the wake and background TLS are the same. Figs. 22 and 23 show the radial evolution obtained from this extraction for the turbulent variables:

The background TI (Fig. 20) slowly increases from the bypass hub up to the casing where it suddenly increases because of the boundary layer. Nevertheless, it should be noticed that the background TI does not display a sudden increase close to the bypass hub. This is due to the fact that the extrapolation process does not take the presence of the bypass hub into account, leading also to a non-zero velocity at this position (see Fig. 17). In the wake, the turbulence intensity is larger (Fig. 21). The turbulence intensity decreases from the hub up to 20% of the stator span and then starts to increase. The wake turbulence intensity reaches its peak at around 95% of the stator span where the wake seems to significantly interact with the tip-gap flow, as seen in Fig. 18. Regarding the TLS, the two estimates give quite similar results up to 80% of the stator height. Above 80%, the TLS decreases for the k-ω based estimate whereas the estimate from Jurdic *et al.*increases close to the casing. This is due to the fact that the closer to the casing the wake is, the larger it gets because of its interaction with the tip-gap flow. This results in a higher estimate for Jurdic's formulation.

C. Analytical Model Results

Two models representing the state of the art of analytical broadband RSI noise prediction have been applied to predict the noise: the model of Hanson [13], and the model of Posson [2, 14, 15] as implemented in the *Optibrui* platform, jointly developed by Université de Sherbrooke, Ecole Centrale de Lyon, Airbus, Technofan and Valeo. Both

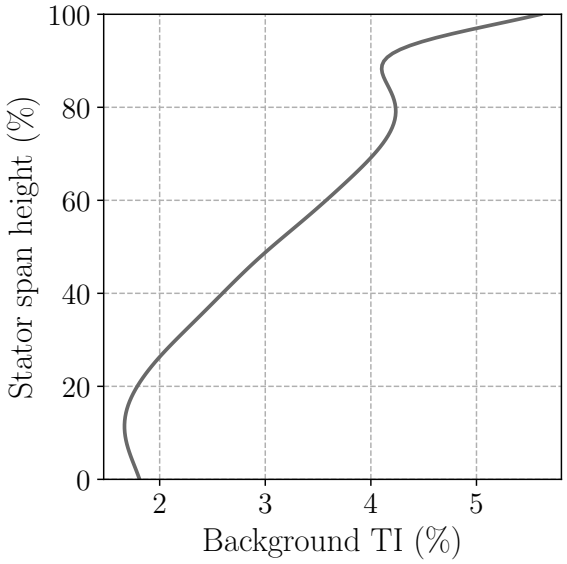

Figure 20 Radial evolution of the TI in the background flow.

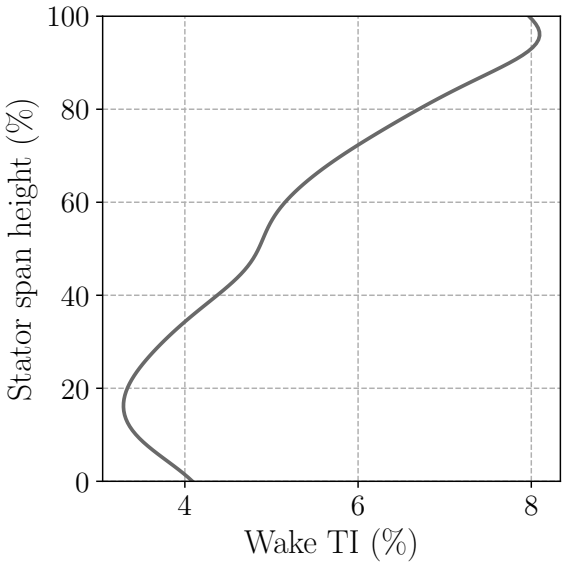

Figure 21 Radial evolution of the TI in the wake.

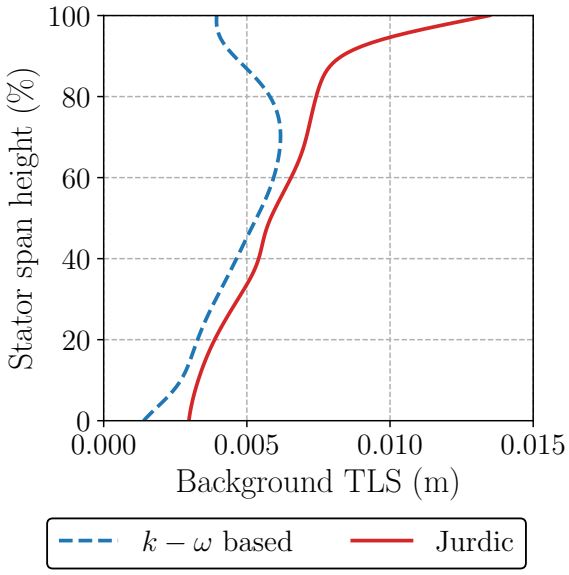

Figure 22 Radial evolution of the TLS in the background flow.

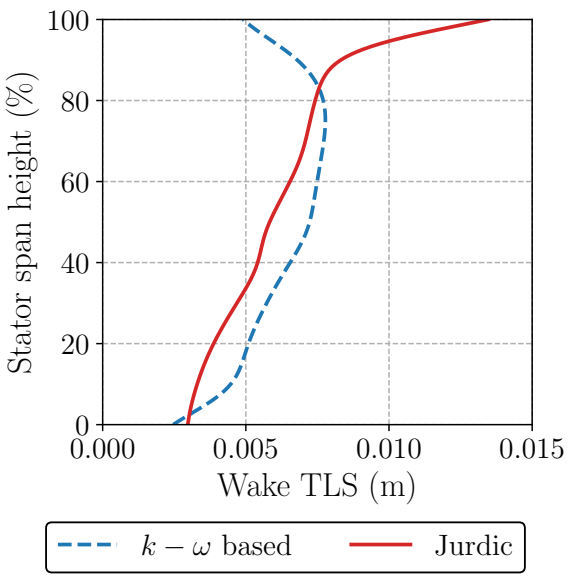

Figure 23 Radial evolution of the TLS in the wake.

models are based on Glegg's cascade response [16] and resort to the strip theory in which the stator is divided into several strips. Each strip corresponds to Glegg's configuration in which a rectilinear cascade of zero-thickness flat plates of infinite span is subject to a 3D impinging gust. The two models mainly differ in the way the acoustic propagation is modeled. In Hanson's model, the propagation is performed in the free space accounting for mean axial flow whereas in Posson's model, the unsteady loading is used as an equivalent dipole source within an in-duct analogy (Goldstein's

analogy [5]) taking into account a uniform axial flow and distributing the acoustic energy over the duct cut-on modes.

The experimental acoutic power level (PWL) displayed in the following result comparisons have been computed using the microphone measurements. The upstream PWL obtained from the forward arc was computed by integrating the sound pressure spectra measured by the far-field microphones weighted by the sine of the radiation angle. The downstream PWL was computed using the pressure signals at the casing of the bypass section by assuming a particular energy distribution over the acoustic cut-on modes. This method is referred to as Wave Number Decomposition (WND) and is detailed in Tapken *et al.*[17].

The input parameters, presented in the previous section, have been used to inform both models in order to carry out broadband noise predictions. Figs. 24 and 25 show the prediction for both noise models using both integral length scale estimates. The way the integral length scale is computed has a significant impact on the radiated noise for both models, especially at low frequency. Indeed, as seen in Figs. 22 and 23, larger turbulent structures are found at the tip of the stator with Jurdic's estimate, which eventually leads to higher noise levels at low frequency. The gap between the two approaches can reach values up to 7 dBs for Posson's model and 4 dBs for Hanson's model. This means that it is paramount to correctly simulate the tip-gap flow and to determine which TLS estimate is the most reliable when retrieving data from RANS simulations. As also shown by Leonard *et al.*in the NASA Source Diagnostic Test case (SDT) [1], the power spectra obtained with Jurdic's approach are closer to the experimental data in terms of shape and absolute values. This makes sense since the casing region is a region of highly unsteady and intermittent flow where turbulence is neither isotropic nor at equilibrium : therefore the k-ω based length scale estimate is not expected to be representative in the casing region, especially in the tip flow wake, whereas the Jurdic estimate, although obtained with the same turbulence model, is based on a wake width that also takes into account large scale mixing.

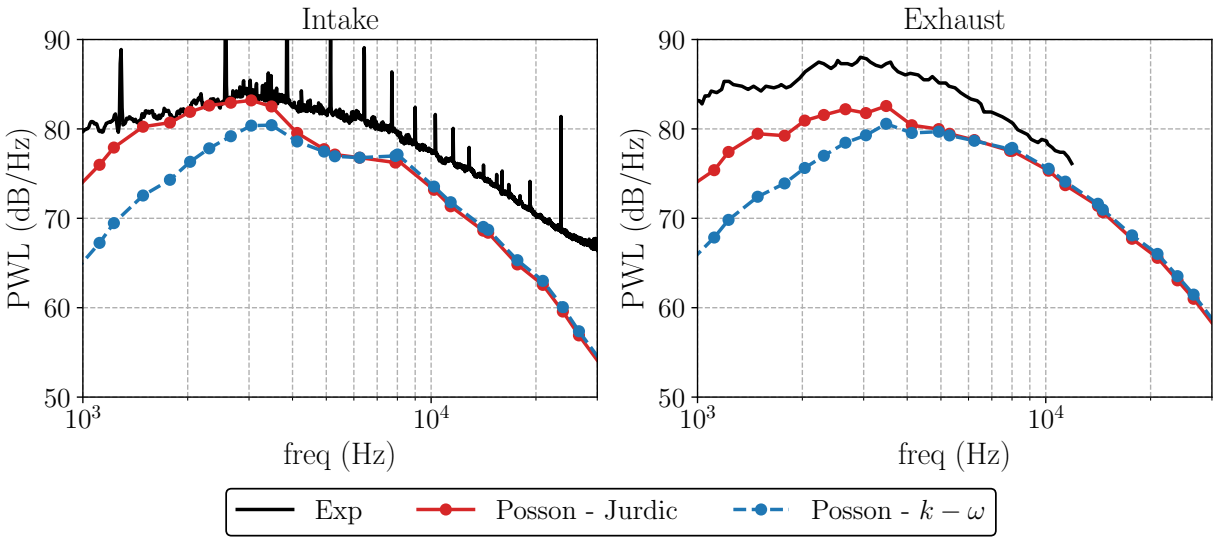

Figure 24 Upstream PWL (left) and Downstream PWL (right) spectra predicted by Posson's model.

Figure 26 shows a comparison between the radiated broadband acoustic power predicted by the two models, using Jurdic's approach for the TLS.

For the upstream predictions, Posson's model underestimates the noise levels from 1kHz up to 1.5kHz but gives fairly good estimates from 1.5kHz up to 3.5kHz. From that point, Posson's model underestimates the acoustic power with a gap ranging from 2 dBs up 12 dBs for the highest frequencies. Hanson's model underestimates the noise levels on the entire frequency range with an almost constant gap with the experiment of 2.5 dBs from 1 kHz up to 5kHz. Above this frequency, the disparities with the experimental data progressively increase to reach a maximum value of 7 dBs. Between 4kHz up to 15kHz, the two models give very similar results. Hanson's model recovers quite faithfully the shape of the experimental PWL.

For the downstream predictions, Posson's model underestimates the acoustic power on the studied frequency range with

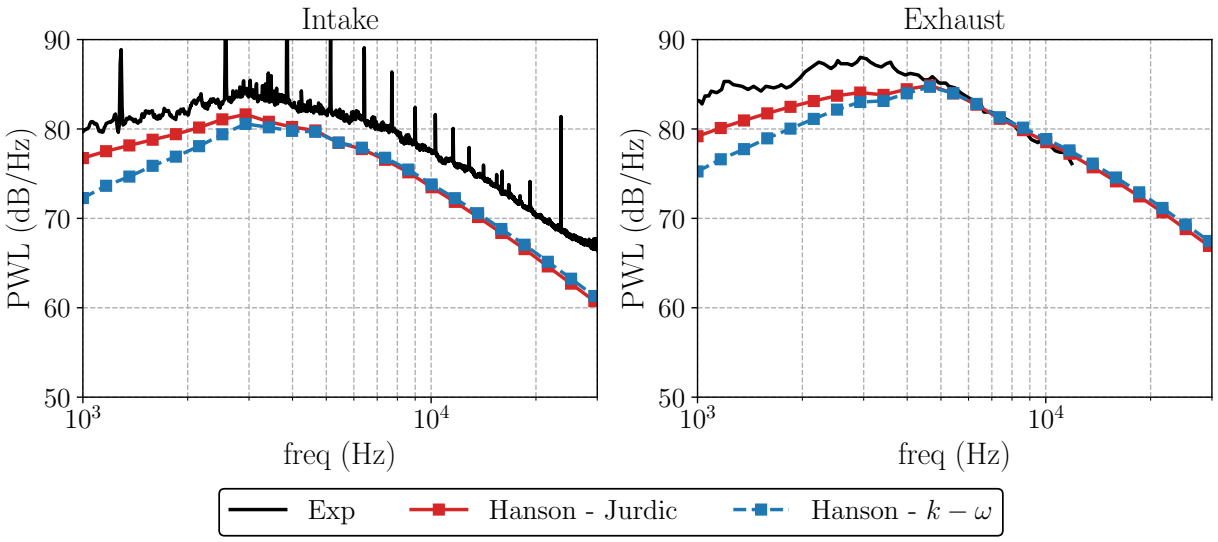

Figure 25 Upstream PWL (left) and Downstream PWL (right) spectra predicted by Hanson's model.

a maximum gap of 9 dBs with the experiment at very low frequencies. The discrepancies then progressively decrease down to 3 dBs at 12 kHz. The overall shape of the spectra is very similar to the experimental one. The PWL obtained from Hanson's model displays higher levels than Posson's model on the entire frequency range. A discrepancy of about 3-4 dBs is observed with the experiment between 1kHz and 4kHz. Above this frequency, the prediction overlays the experimental results.

A few conclusions can be drawn from these observations. First of all, as observed by Leonard *et al.*[1] in the SDT case, Posson's model produces lower noise estimates than Hanson's model, especially at low frequencies because of the duct cut-off effect. This phenomenon is easily noticeable for the downstream predictions. For the upstream predictions, however, this phenomenon only appears for frequencies below 1.1kHz, meaning that the cut-off modes are not those which transport the dominant part of the acoustic energy.

Secondly, previous studies of the SDT case [1] have shown that the model of Hanson tends to slightly overestimate the downstream PWL, especially at low frequencies. They also showed that Posson's model underestimates the noise radiated downstream of the stator. However, the gap between the experiment and the prediction did not exceed 5 dBs when using Jurdic's TLS estimate.

The unexpected discrepancies found in the ACAT1 case may originate from several phenomena:

- The RSI mechanism may not be the only mechanism responsible for broadband noise production in the present ACAT1 configuration. Other mechanisms, such as the flow detachment at the rotor LE, or the tip noise resulting from the interaction of the casing boundary layer with the rotor, may contribute to the rotor self noise and may not be negligible. The fact that the models underestimate the noise, whereas the TKE levels are substantially higher than in the experiment, tends to confirm this point. In addition, some blade-to-blade variations have been observed in the measured wakes (Figs. 12a-15a at around 3 o'clock), which strongly suggests that some noise components are present in the experiment which are due to hardware design issues.
- The model assumptions may not be completely correct in the specific case of the ACAT1 configuration.

All these points will be investigated in an upcoming study using Large Eddy Simulation to investigate more precisely the unsteady phenomena of this configuration. It should also be noted that not all the phenomena of the RSI mechanisms are taken into account. For instance, the rotor masking effect as well as the swirl flow upstream of the stator have not been taken into account and may have a significant influence on the PWL as shown by Posson *et al.*[18] and Masson *et al.*[3].

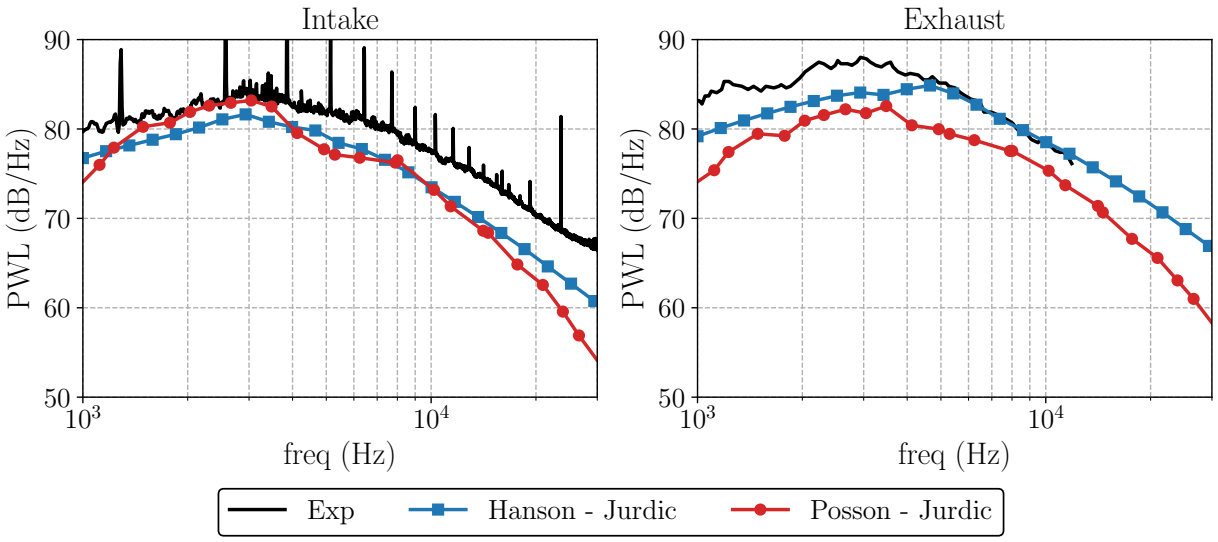

Figure 26 Comparison of the PWL obtained from the model of Hanson and the model of Posson.

VII. Conclusion

A comprehensive noise computation of the ACAT1 configuration at approach condition has been performed using RANS-informed analytical models. The RANS simulation is in excellent agreement with the performance parameters but shows some disparities with the hot-wire measurements, especially regarding the turbulence kinetic energy which seems to be overestimated by the simulation and not fully periodic in the experiment. The impact of the turbulent length scale estimate on the PWL has been studied, showing PWL shapes and absolute values in better agreement with the experiment when using Jurdic's approach than when using the k-ω based estimate. Both Hanson's and Posson's models underestimate the noise levels on a large part of the studied frequency range. This underestimation may be attributed to additional broadband noise sources which may not be negligible with respect to the RSI mechanism. The model assumptions might also not be correct in the specific case of the ACAT1 configuration. Further analysis through Large Eddy Simulation is needed to fully understand the discrepancies observed in the noise predictions.

Acknowledgments

The presented work was conducted in the frame of the project TurboNoiseBB, which has received funding from the European Union's Horizon 2020 research and innovation program under grant agreement No. 690714.
It was also performed within the framework of the Labex CeLyA of the Université de Lyon, within the program "Investissements d'Avenir" (ANR-10-LABX-0060/ANR-16-IDEX-0005) operated by the French National Research Agency (ANR)
The authors want to thank all the participants to the test campaign, especially Wolfram Hage (DLR), Karsten Liesner and the team of AneCom AeroTest, Wolfgang Weith and Nick Crowder (Rolls-Royce), Azucena Pintado and Thomas Nodé-Langlois (AIRBUS). The upstream far-field acoustic power spectrum was provided by Azucena Pintado. The downstream acoustic power spectrum was provided by Maximilian Behn (DLR).
The authors acknowledge the provision of the hotwire data by Robert Meyer and Sebastian Hakansson (DLR).
The authors are very grateful to Marlène Sanjosé (Université de Sherbrooke), for her precious advice about analytical models and for her continued support on the use of the OPTIBRUI platform and the pre-processing tools.
The authors also want to thank Gabriele Grasso (Ecole Centrale de Lyon) for his expertise in wake extrapolation and for providing his implementation of the Jaron's method, and Sébastien Guérin (DLR) for his advice on the input parameters for the method.
Most of the RANS post-processing was performed using Antares (release 1.13.0, https://www.cerfacs.fr/antares).

References

[1] Leonard, T., Sanjose, M., Moreau, S., and Duchaine, F., "Large Eddy Simulation of a scale-model turbofan for fan noise source diagnostic," *22nd AIAA/CEAS Aeroacoustics Conference*, 2016, pp. 1–23. doi:10.2514/6.2016-3000, URL http://arc.aiaa.org/doi/10.2514/6.2016-3000.

[2] Posson, H., Moreau, S., and Roger, M., "On the use of a uniformly valid analytical cascade response function for fan broadband noise predictions," *Journal of Sound and Vibration*, Vol. 329, No. 18, 2010, pp. 3721–3743. doi:10.1016/j.jsv.2010.03.009.

[3] Masson, V., Posson, H., Sanjose, M., Moreau, S., and Roger, M., "Fan-OGV interaction broadband noise prediction in a rigid annular duct with swirling and sheared mean flow," *22nd AIAA/CEAS Aeroacoustics Conference, 2016*, 2016, pp. 1–18. doi:10.2514/6.2016-2944.

[4] Williams, J. E. F., and Hawkings, D. L., "Sound Generation by Turbulence and Surfaces in Arbitrary Motion," *Philosophical Transactions of the Royal Society A: Mathematical, Physical and Engineering Sciences*, Vol. 264, No. 1151, 1969, pp. 321–342. doi:10.1098/rsta.1969.0031, URL http://rsta.royalsocietypublishing.org/cgi/doi/10.1098/rsta.1969.0031.

[5] Goldstein, H., "Aeroacoustics," *Nasa Report SP-346*, 1974, pp. 1–440. URL http://ntrs.nasa.gov/archive/nasa/casi.ntrs.nasa.gov/19740027005.pdf.

[6] Cader, A., Polacsek, C., and Garrec, T. L., "Numerical prediction of rotor-stator interaction noise using 3D CAA with synthetic turbulence injection," *2018 AIAA/CEAS Aeroacoustics Conference*, 2018, pp. 1–17. doi:10.2514/6.2018-4190.

[7] Bailly, C., and Juve, D., "A stochastic approach to compute subsonic noise using linearized Euler's equations," *5th AIAA/CEAS Aeroacoustics Conference and Exhibit*, , No. I, 1999, pp. 496–506. doi:10.2514/6.1999-1872, URL http://arc.aiaa.org/doi/10.2514/6.1999-1872.

[8] Bailly, C., and Lyon, E. C. D., "Numerical Solution of Acoustic Propagation Problems Using Linearized Euler Equations," *AIAA Journal*, Vol. 38, No. 1, 2000, pp. 22–29. doi:10.2514/2.949.

[9] Guérin, S., Kissner, C., Kajasa, B., Jaron, R., Behn, M., Hakansson, S., Pardowitz, B., Tapken, U., Meyer, R., and Enghardt, L., "Noise prediction of the ACAT1 fan with a RANS-informed analytical method: success and challenge," *submitted to: 25th AIAA/CEAS Aeroacoustics Conference 2019*, 2019.

[10] Jaron, R., Moreau, A., and Guerin, S., "Extrapolation of RANS flow data for improved analytical fan tone prediction," *21st AIAA/CEAS Aeroacoustics Conference*, American Institute of Aeronautics and Astronautics, Reston, Virginia, 2015, pp. 1–19. doi:10.2514/6.2015-2515, URL http://arc.aiaa.org/doi/10.2514/6.2015-2515.

[11] Pope, S. B., *Turbulent Flows*, 2001. doi:https://doi.org/10.1017/CBO9780511840531.

[12] Jurdic, V., Joseph, P., and Antoni, J., "Investigation of Rotor Wake Turbulence Through Cyclostationary Spectral Analysis," *AIAA Journal*, Vol. 47, No. 9, 2009, pp. 2022–2030. doi:10.2514/1.36728, URL http://arc.aiaa.org/doi/10.2514/1.36728.

[13] Hanson, D. B., "Theory for broadbad noise of rotor & stator cascades with inhomogenous inflow turblence including effects of lean and sweep," , No. May, 2001, p. 86.

[14] Posson, H., Roger, M., and Moreau, S., "On a uniformly valid analytical rectilinear cascade response function," *Journal of Fluid Mechanics*, Vol. 663, 2010, pp. 22–52. doi:10.1017/S0022112010003368, URL http://www.journals.cambridge.org/abstract{_}S0022112010003368.

[15] Posson, H., Moreau, S., and Roger, M., "Broadband noise prediction of fan outlet guide vane using a cascade response function," *Journal of Sound and Vibration*, Vol. 330, No. 25, 2011, pp. 6153–6183. doi:10.1016/j.jsv.2011.07.040, URL http://dx.doi.org/10.1016/j.jsv.2011.07.040.

[16] Glegg, S. A., "The response of a swept blade row to a three-dimensional gust," *Journal of Sound and Vibration*, Vol. 227, No. 1, 1999, pp. 29–64. doi:10.1006/jsvi.1999.2327, URL http://linkinghub.elsevier.com/retrieve/pii/S0022460X99923271.

[17] Tapken, U., Behn, M., Spitalny, M., and Pardowitz, B., "Radial mode breakdown of the ACAT1 fan broadband noise generation in the bypass duct using a sparse sensor array," *submitted to: 25th AIAA/CEAS Aeroacoustics Conference 2019*, 2019.

[18] Posson, H., and Moreau, S., "Effect of Rotor Shielding on Fan-Outlet Guide Vanes Broadband Noise Prediction," *AIAA Journal*, Vol. 51, No. 7, 2013, pp. 1576–1592. doi:10.2514/1.j051784.